minerals

MDPI

Article

Trace Elements in Pyrite and Its Crystallization Temperature: An Example of Gold Deposits in the Darasun Goldfield, Eastern Transbaikalia, Russia

Vsevolod Prokofiev [1,*], Valeriya Brovchenko [1], Lidiya Zorina [2], Anton Krasnov [3], Vera Abramova [1] and Nikolay Bortnikov [1]

[1] Institute of the Geology of Ore Deposits, Petrography, Mineralogy, and Geochemistry (IGEM), Russian Academy of Sciences, 109017 Moscow, Russia
[2] Vinogradov Institute of Geochemistry, Siberian Branch, Russian Academy of Sciences, 664033 Irkutsk, Russia
[3] Central Research Exploration Institute for Base and Precious Metals, 117549 Moscow, Russia
* Correspondence: vpr@igem.ru

Abstract: The distributions of trace elements in pyrite were studied in samples of high-grade gold ores from the Talatui, Teremkyn, and Darasun deposits. The paper presents LA-ICP-MS data on concentrations of trace elements in pyrite in gold ores from mineral deposits of the Darasun goldfield, which were produced by a single fluid–magmatic system at various temperatures. The high-temperature pyrite was found to be enriched in Co, Se, and W, whereas the medium-temperature pyrite was enriched in Cu, Zn, Ag, Te, As, and In. The behaviors of some elements (Ni, Au, Bi, Sb, and Pb) seem to be independent of temperature. The identified trends and relations in the behaviors of elements can be used in studying the Au-Bi mineralization of the intrusion-related type.

Keywords: trace elements; pyrite; gold deposits; temperature

Citation: Prokofiev, V.; Brovchenko, V.; Zorina, L.; Krasnov, A.; Abramova, V.; Bortnikov, N. Trace Elements in Pyrite and Its Crystallization Temperature: An Example of Gold Deposits in the Darasun Goldfield, Eastern Transbaikalia, Russia. *Minerals* **2023**, *13*, 288. https://doi.org/10.3390/min13020288

Academic Editors: Vladimir Tauson and Sergey Lipko

Received: 23 January 2023
Revised: 15 February 2023
Accepted: 17 February 2023
Published: 18 February 2023

1. Introduction

Pyrite is one of the most widely spread minerals at various hydrothermal ore deposits. This mineral can provide valuable information on the ore-forming processes reflected in some features of the distributions of trace elements in it (e.g., [1–7]). The technique of laser ablation–mass spectrometry with inductively coupled plasma (LA-ICP-MS) makes it possible to highly accurately study the minor- and trace-element compositions of various minerals. Information thus recovered was used by many researchers in resolving a wide area of geological problems, including elucidation of the possible sources of metals, evolution of hydrothermal fluids, and mechanisms able to form mineral deposits [8–17].

This study is focused on the distribution patterns of admixture elements in pyrite from auriferous veins and mineralization zones at the Darasun goldfield. These deposits were formed at different temperatures in various parts of the single fluid–magmatic system [18].

The Darasun goldfield has a very long exploration history. The gold placer has been known since 1861. The first yields of gold-bearing quartz-sulfide vein of 1900 m length were found in 1883, which marked the beginning of the Darasun gold deposit. Gold was extracted by washing from the fractured vein material. Later, oxidized sulfide ores were extracted by underground mining at depths of 35–50 m. As the mines deepened, the degree of oxidation of the ores decreased, up to the appearance of unchanged sulfide ores.

Since the systematic study of the region's geological structure was started in 1927, one after another, new gold veins of Darasun deposit were discovered. There turned out to be more than 200. It became clear the deposit is large. Intensive mining of Darasun took place in the period from 1934 to 1954. In the mid-1970s, the main lodes were depleted, and exploitation of the deposit has become less intensive. However, during the study of the district, the Teremkyn deposit was discovered in 1971 and the Talatui one in 1974.

2. Geological Background

The Darasun, Teremkyn, and Talatui gold mines are located in the Chita area of the eastern Transbaikalian region, 70 km southwest of the Mongolian-Okhotsk suture zone generated by the collision between the Mongolian and Siberian continents in the latest Mesozoic. The tectonic evolution of the region is complicated by a sequence of thrusting, folding, and magmatic episodes that lasted for about 50 m.y., from the Early and/or Middle Jurassic to the end of the Jurassic. The Darasun goldfield has been known for more than a century and comprises three mineral deposits: the large Darasun gold deposit, the medium-sized Talatui gold deposit, and the small Teremkyn deposit, as well as several occurrences of auriferous mineralization. The Darasun goldfield is a mining district in Transbaikalia, Russia that is of relevant geologic and economic importance [18,19]. The district is named after the largest deposit of the region, the Darasun gold mine, which was under exploration for more than a century [19]. Darasun was discovered in 1861 and produced 118 metric tons (t) from underground operations and an additional 40 t from surface (gold placer) operations. Long-term studies in the field have proved its gold deposits were produced by a single magmatic–fluid mineral system of the Jurassic age, which was related to the emplacement of granodiorite porphyry of the Amudzhikan–Sretenskii complex [19,20]. This ore field is hosted in Paleozoic magmatic rocks, mostly of mafic composition (Figure 1). The deposits occur at different distances from the granitoid intrusion of the Amudzhikan–Sretenskii complex, which was dated at 160.5 ± 0.4 Ma, and the age of the wall-rock metasomatites at the Darasun deposit is 159.6 ± 1.5 Ma [21], i.e., the ore-forming hydrothermal process that produced the Au mineralization was correlated in age with the magmatic process.

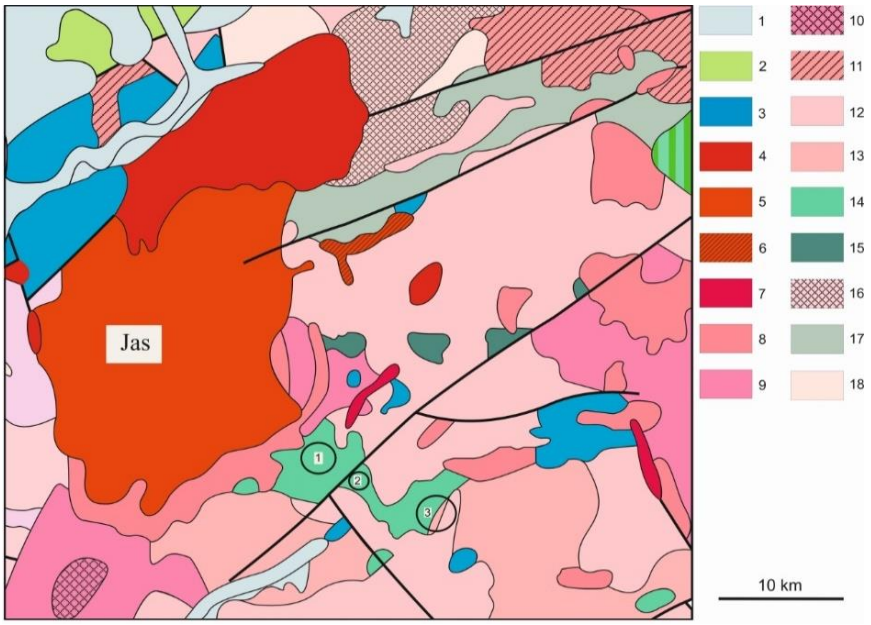

Figure 1. Schematic geologic map of the Darasun district and its vicinities [22]. (1) Quaternary; (2) Upper Turga subseries (K1tr2): sandstone, siltstone, mudstone, conglomerate, basaltic andesite, trachybasalt, rhyolite, tuff, tuffaceous rocks, and coal; (3) Nerchinsk poorly defined series (J3nr): latite, quartz latite, trachybasalt, trachyandesite, trachyrhyodacite, rhyolite, trachirhyolite, tuff, conglomerate, sandstone, siltstone, and tuffaceous rock; (4) Dotulur complex (γJ3d): leucogranite, pegmatoid granite, and amazonite granite; (5–7) Amudzhikan–Sretensky complex (qξ2J3as): (5) phase-II quartz syenite, (6) phase-II granodiorite porphyry, (7) phase-II granite porphyry; (8–10) Amanan complex (γ2J2-3a): (8) phase-II granite (γ) and aplite-like granite, (9) phase I quartz syenite (qξJ2-3a), (10) phase I granodiorite (γδ1J2-3a); (11) Bichura complex, phase III (γ3P2b): leucogranite, granite, porphyry granite,

and quartz syenite; (12) Olyokma complex (γPZ1o): granite; (13) Krestovsky complex (γδPZ1kr): granodiorite, quartz diorite, diorite, quartz syenite, tantalite, and plagiogranite; (14, 15) Kruchina complex (νδ1PZ1k): (14) gabbro, (15) gabbrodiorite; (16) Late Stanovoy complex (γδ2PR1ps): granodiorite; (17) Oloshka complex (δPR1o): diorite; and (18) Tungir complex (qPR1t): gneiss and migmatite. Circles are gold deposits: (1) Talatui, (2) Teremkyn, and (3) Darasun.

The Talatui deposit with stringer and disseminated gold mineralization is hosted in gabbroids of the Kruchininskii complex and is the closest to the intrusive granitoid body of the Amudzhikan–Sretenskii complex, whereas the auriferous veins of Teremkyn and Darasun deposits are located 7 and 12 km, respectively, southeast of this body. The Teremkyn deposit is hosted in gabbroic rocks of the Kruchininskii complex. The Darasun deposit occurs at the contact between gabbroids of the Kruchininskii complex and granitoids of the Krestovskii one. The different distances between the two deposits and the granitoid massif of the Amudzhikan–Sretenskii complex are well seen on the map.

Three stages (early, productive mineral, and late) have been recognized in formation of deposits in the Darasun goldfield, and the bulk of gold was deposited during the second (productive) stage [18,19,23,24]. The three deposits in the Darasun gold field have many similarities in that the dominant minerals of the ores are quartz, pyrite, pyrrhotite, tourmaline, bismuth and tellurium minerals, and native gold. At the same time, the deposits display several differences [18]. The mineral compositions of the ores become more complicated from the Talatui to Darasun deposits. For example, the mineralogy of the Talatui deposit ores is relatively simple (pyrite, magnetite, chalcopyrite, tourmaline, plus some very rare bismuth and tellurium minerals), while the Teremkyn deposit contains more various minerals, tourmaline and quartz are more abundant, and the veins contain arsenopyrite, galena, sphalerite, fahlores, and abundant bismuth mineralization. The ores at the Darasun deposit are the most complicated (they contain much arsenopyrite, antimony and bismuth sulfosalts, tellurides, and various rare minerals). Differences were also found between the morphologies of the orebodies, ore structures, the mineralogy of the ores and metasomatic rocks within this ore field, which may be explained by variations in the physicochemical parameters of the ore-forming processes (e.g., [18,25]). The chemistry of native gold in the various deposits is also different (Figure 2). The content of Au is at a maximum in the stringer and disseminated ores at the Talatui deposit (99.8–67.3 at. %) and is somewhat lower at Teremkyn (88.1–51.0 at. %), whereas native gold in veins at the Darasun deposit is the richest in silver (content of Au 83.4–57.0 at.%). At all deposits, native gold and pyrite aggregates were often deposited during the productive (mineral) stages (Figure 3). These aggregates are commonly interpreted as evidence of the simultaneous crystallization of native gold and pyrite (e.g., [19]), and hence, information on the trace-element composition of the pyrite may shed light onto some details of the crystallization of the gold.

Fluid inclusion studies [18,20,25,26] have uncovered significant differences in the temperatures of mineral deposition at the deposits (Figure 4). The veins at the Darasun deposits were deposited at relatively low temperatures (429–118 °C), the ores of the Teremkyn deposit were formed at temperatures of 466–118 °C, and the stringer and disseminated ores of the Talatui deposit were produced at even higher temperatures of 611–32 °C. Fluid inclusions in ore quartz show evidence of heterogenization (boiling), but it is not possible to compare the scale of this process at the various deposits. The isotopic study of oxygen, carbon, and sulfur isotopes in carbonates, quartz, pyrite, arsenopyrite, and chalcopyrite from the Darasun deposit indicate the mineralizing fluids at the Darasun deposits were of a magmatic nature [27], which is consistent with the hypothesis that the Darasun, Teremkyn, and Talatui deposits were produced by the single fluid–magmatic system [28]. This is also consistent with interpretations that they belong to the intrusion related Au–Bi type deposits [18]. It has been found the temperature ranges of the ore-forming processes widen, and the temperatures at which these processes began become higher with decreasing distance from the intrusion bodies (possibly, magma chamber), and the composition of the mineralizing fluid systematically changed from the high-temperature-deposited veinlets

and disseminated ores of the Talatui deposit to the medium-temperature-formed veins of the Darasun deposit. The mineralizing fluid of the veinlets and disseminated ores at the Talatui deposit was richer in weakly volatile compounds (Cl, SO_4^{2-}, Ca, Br, Sr, etc.), whereas the medium-temperature fluid of the ore veins at the Darasun deposit was relatively enriched in mobile and volatile components (CO_2, CH_4, HCO_3^-, As, Hg, Te, Se, Li, etc.) [29].

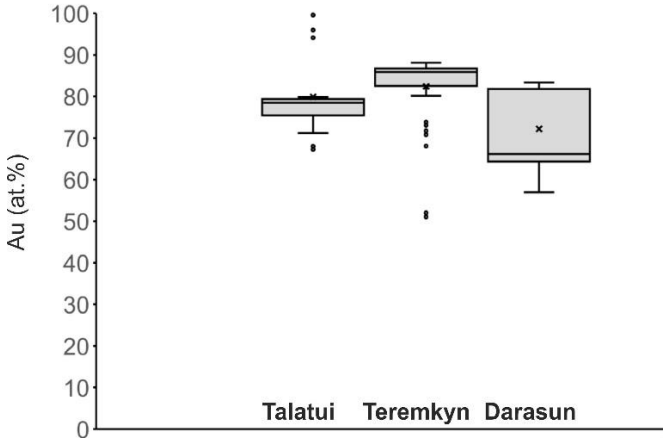

Figure 2. Concentrations of Au (at. %) in native gold in the gold ores at deposits of the Darasun goldfield (recalculated data from [18]). Here and in Figures 4 and 10–12, lines in the boxes are medians, crosses are averages, and spots are outliers (https://towardsdatascience.com/understanding-boxplots-5e2df7bcbd51).

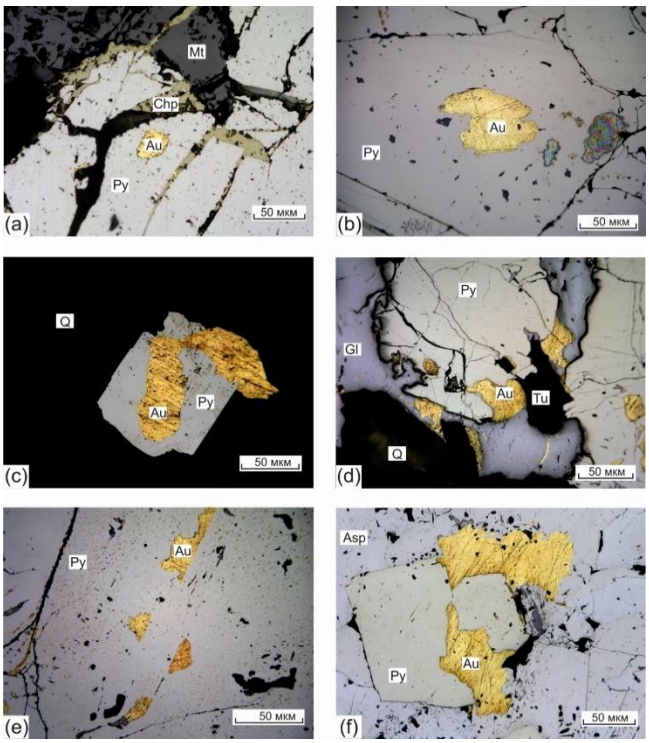

Figure 3. Intergrowths of pyrite and native gold in the ore of the gold deposits: (**a**,**b**) Talatui, (**c**,**d**) Teremkyn and (**e**,**f**) Darasun. Au, native gold; Py, pyrite; Asp, arsenopyrite; Chp, chalcopyrite; Mt, magnetite; Tu, tourmaline; Q, quartz.

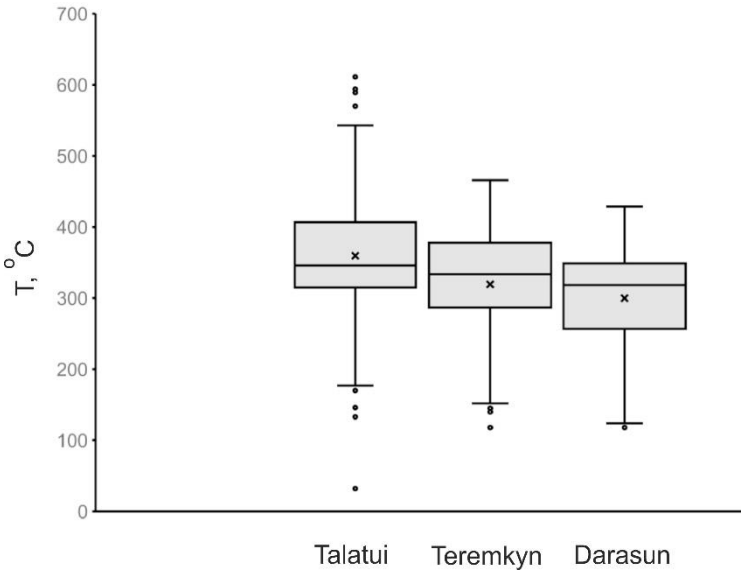

Figure 4. Homogenization temperature of fluid inclusions in quartz of gold ores of deposits of the Darasun goldfield. The figure format is the same as in Figure 2.

Variations in the chemical composition of mineralizing fluids at the Darasun goldfield were closely interrelated with variations in the parameters of ore deposition, depending on the distance from the granitoid intrusive body and physical properties of the fluid, with temperature being the primary factor. Fluid near the magmatic body boiled and segregated into immiscible brine and a less dense phase, which migrated to deep levels more distant from the sources of the fluid and ore components. Because of this, the fluid became richer in relatively volatile components away from the central part of the system. The high-temperature region of the system near the magma chamber was enriched in less mobile volatile components. Thus, variations in the composition of the fluids when the Darasun deposit was produced can be explained by the operation of a single hydrothermal system, which predetermined the geochemistry of the ores and minerals in various parts of this system. It is thus reasonable to expect notable differences between concentrations of admixture elements in pyrite at the three deposits. These results are presented below.

3. Materials and Methods

The distributions of trace elements in the pyrite were studied in samples of high-grade gold ores from the Talatui, Teremkyn, and Darasun deposits. Data from microscopic studies available for these deposits indicated the pyrite contained native gold (Figure 3). However, the analyzed pyrite did not contain segregations of either native gold or other minerals. We studied seven samples of the high-temperature stringer–disseminated ore from the Talatui deposit (which were formed at temperatures of 600–400 °C), two samples of the vein medium-temperature ore of the Teremkyn deposit (produced at 466–250 °C), and seven samples of the vein medium-temperature ore of the Darasun deposit (430–200 °C).

Electron probe microanalysis (EPMA) of pyrite was carried out on a Camebax SX 100 X-ray microprobe at the Vernadsky Institute of Geochemistry and Analytical Chemistry, RAS (analyst N.N. Kononkova). The current was 30 nA, and the accelerating voltage was 20 kV. The measurements were done according to the following analytical lines: PbM_α, SK_α, BiMα, AgLα, AuLα, ZnK_α, FeK_α, CdL_α, MnK_α, CuK_α, HgL_α, and SeL_α; the beam diameter was 2–5 μm. The detection limit is 0.02 wt %; and the measurement uncertainty was ±2 % for major elements and ~20% for trace elements. RAR corrections were used.

Concentrations of trace elements ^{33}S, ^{55}Mn, ^{57}Fe, ^{59}Co, ^{60}Ni, ^{63}Cu, ^{66}Zn, ^{69}Ga, ^{72}Ge, ^{75}As, ^{107}Ag, ^{111}Cd, ^{115}In, ^{118}Sn, ^{121}Sb, ^{125}Te, ^{182}W, ^{197}Au, ^{202}Hg, ^{208}Pb, and ^{209}Bi in sulfides were determined by LA-ICP-MS at IGEM-Analitika. At least 28–152 in-situ LA-ICP-MS analyses of trace elements in pyrite were obtained to compare the Darasun, Teremkyn,

and Talatui ores and are presented in Supplementary Table S1. The LA-ICP-MS system consisted of a New Wave UP-213 solid state Nd:YAG laser coupled to a Thermo XSeries2 quadrupole ICP-MS. Calibration was performed using USGS-certified reference material MASS1. The artificial sulfide reference material UQAC-FeS-1 [30], which is produced at UQAC based on a modified technique developed by [31], was used to monitor data quality.

The accuracy (marked as E % in Table S2) of the analysis was generally <20% and was calculated as the relative difference between the average individual SRM measurement and the known concentration in the reference material (Table S2). The precision of the measurements is reported as a relative standard deviation (RSD) for each element, calculated as the standard deviation divided by the average concentration (Table S1). The relative standard deviation was <20%. The results of the SRM measurements of all sessions and the detection limits for each element are given in Supplementary Table S2.

LA-ICP-MS analyses were conducted using a beam 80 μm in diameter for spots and 50 μm for lines, a laser frequency of 15 Hz, 5–7 J/cm^2 energy density, and 7 μm/s ablation speed for lines. The carrier gas was a mixture of helium (0.7 L/min) and argon (0.85 L/min). The acquisition time in the spot mode was 30 s for the backgrounds, 60 s for the mineral analysis, and 30 s for washout. Each line profile was preceded by 30 s of background. The material was analyzed using ICP-MS operating in a time-resolved mode, using peak jumping and a dwell time of 10 ms/peak per element. All major and trace elements measurements were carried out using the time-resolved analysis (TRA) mode, which operated in fast, peak jumping mode. Signal quantification was carried out by the Iolite software [32], using ^{33}S as an internal standard. Sulfur concentration was calculated from the stoichiometry of the sulfides. If micro-inclusions of gold, silver, or other minerals were identified in the LA-ICP-MS spectra, the corresponding part of the spectrum was cut out off-line. Minerals in the profiles through intergrowths were calculated separately, avoiding areas around contacts.

4. Results

4.1. EPMA

The EPMA results on pyrite samples from the deposits of the Darasun goldfield are presented in Table 1. The S and Fe contents of the Talatui deposit are 51.51–54.03 wt.% (avg. 53.09 wt.%) and 43.84–46.99 wt.% (avg. 46.01 wt.%), respectively, those at the Teremkyn deposit are 53.00–55.28 wt.% (avg. 54.01 wt.%) and 45.30–47.72 wt.% (avg. 46.76 wt.%), respectively, and those at the Darasun deposit are 51.20–55.23 wt.% (avg. 53.38 wt.%) and 45.64–47.79 wt.% (avg. 46.76 wt.%) (Table 1, Figure 5a), respectively. The Cu and Au contents vary from 0.01 to 0.30 wt.% (avg., 0.09 wt.%) and 0.01 to 1.73 wt.% (avg. 0.29 wt.%) in pyrite of the Talatui deposit, respectively, from 0.01 to 0.37 wt.% (avg. 0.11 wt.%) and 0.01 to 0.71 wt.% (avg. 0.27 wt.%) in pyrite of the Teremkyn deposit, respectively, and from 0.01 to 0.48 wt.% (avg. 0.14 wt.%) and 0.01 to 0.61 wt.% (avg. 0.19 wt.%) in pyrite of the Darasun deposit (Table 1, Figure 5b), respectively. The samples have also been analyzed for As, Co, Ni, Se, Ag, Sb, Te, and Bi, but many analyses by this technique showed concentrations of admixtures below the detection limits (Table 1).

Table 1. Summary of EMPA analyses (wt.%) of pyrite from the gold deposits of the Darasun goldfield.

Parameter	S	Fe	Co	Ni	Cu	As	Se	Ag	Sb	Te	Au	Bi	Total	S/Fe(at)
Talatui														
Max.	54.03	46.99	2.57	0.29	0.30	0.60	1.42	0.16	0.11	0.12	1.73	0.30	101.60	2.10
Min.	51.51	43.84	0.01	0.01	0.01	0.01	0.01	0.01	0.01	0.01	0.01	0.01	98.79	1.95
Mean	53.09	46.01	0.59	0.06	0.09	0.09	0.45	0.06	0.03	0.05	0.29	0.14	100.10	2.01
Median	53.17	46.17	0.30	0.05	0.08	0.04	0.08	0.04	0.03	0.04	0.07	0.14	100.11	2.01
n	111	111	104	66	72	36	28	39	32	36	17	64	111	111
Teremkyn														
Max.	55.28	47.72	0.29	0.96	0.37	1.39	0.06	0.10	0.06	-	0.71	0.24	102.95	2.09

Table 1. *Cont.*

Parameter	S	Fe	Co	Ni	Cu	As	Se	Ag	Sb	Te	Au	Bi	Total	S/Fe(at)
Min.	53.00	45.30	0.10	0.01	0.01	0.02	0.02	0.01	0.01	-	0.01	0.10	99.82	1.97
Mean	54.01	46.76	0.08	0.14	0.11	0.35	0.03	0.05	0.03	-	0.27	0.15	101.40	2.01
Median	53.86	46.60	0.07	0.06	0.09	0.25	0.03	0.06	0.03	-	0.11	0.12	101.82	2.00
n	22	22	16	13	13	16	6	8	9	-	6	8	22	22
Darasun														
Max.	55.23	47.79	1.00	0.10	0.48	1.54	0.02	0.05	0.08	0.11	0.61	0.24	102.73	2.05
Min.	51.20	45.64	0.02	0.01	0.01	0.02	0.02	0.01	0.01	0.01	0.01	0.10	98.61	1.93
Mean	53.38	46.76	0.09	0.04	0.14	0.38	0.02	0.03	0.03	0.06	0.19	0.15	100.69	1.99
Median	53.37	46.65	0.06	0.03	0.07	0.10	0.02	0.04	0.03	0.06	0.12	0.13	100.65	1.99
n	33	33	30	19	20	22	3	3	15	2	10	4	33	33

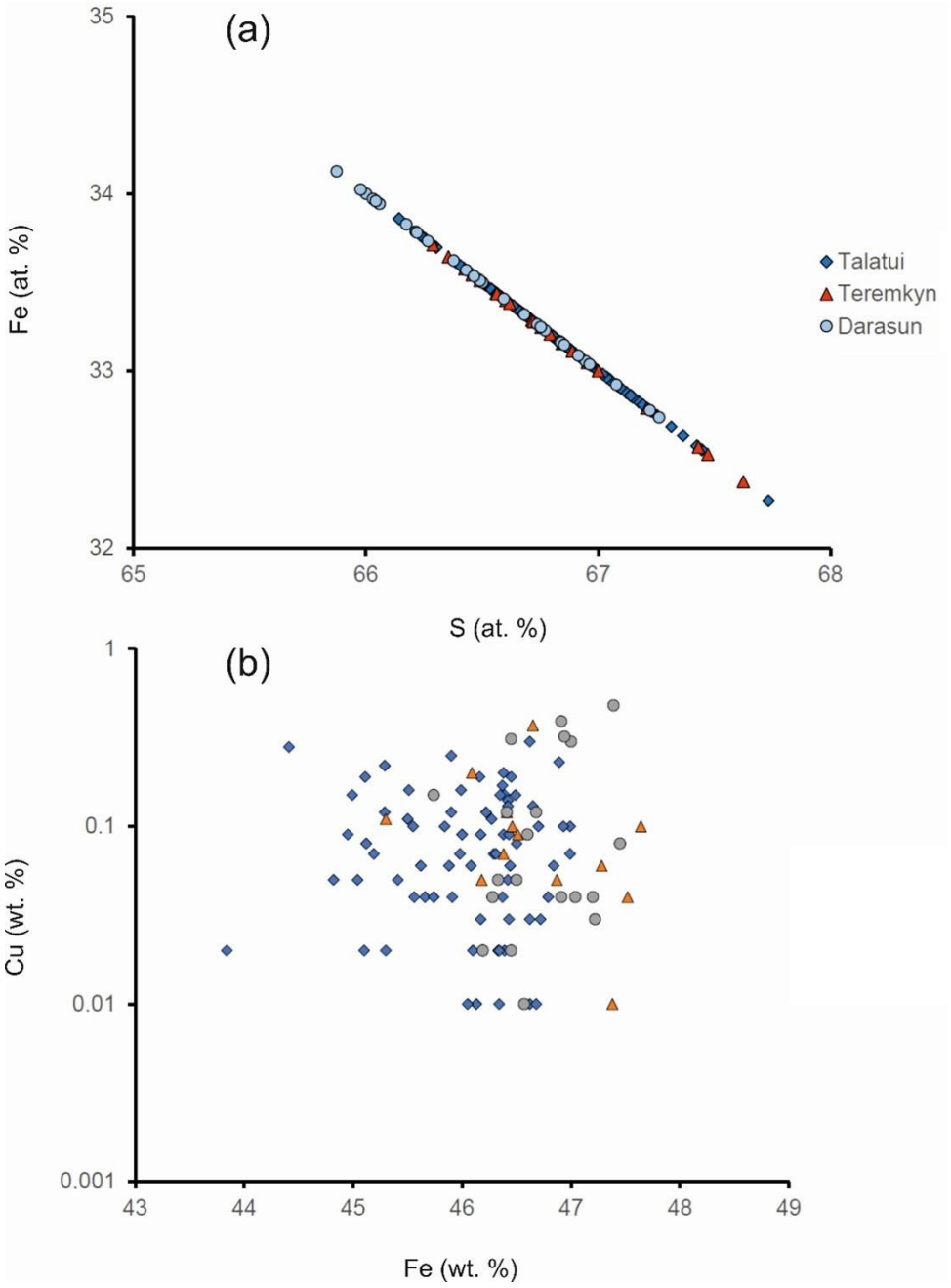

Figure 5. Binary plots of (**a**) Fe vs. S, (**b**) Cu vs. Fe in the pyrite samples from the deposits of the Darasun goldfield. EPMA data.

The S/Fe atomic ratio varies from 2.10 to 1.93 (Table 1), suggesting a deviation of chemical composition of pyrite in the sample studied from the stoichiometric one [33].

4.2. LA ICP MS

The LA-ICP-MS study was conducted with pyrite from the Talatui, Teremkyn, and Darasun deposits. The median and geometric mean as well as the maximum and minimum values of all measurements, are presented in Table 2. Trace elements are heterogeneously distributed within the grains, thus defining various trends and combinations with one another in minerals from the various deposits (Figures 6–8). Cobalt is strongly concentrated in accordance with the temperature range estimated for each deposit. The high-temperature pyrite from the Talatui deposit contains up to 20,559 ppm of Co (median 541.5 ppm), whereas a middle-temperature pyrite from Teremkyn contains up 5607 ppm, and pyrite from Darasun bears up to 3231 ppm Co (Figures 6 and 7A; Table 2). Arsenic contents also vary over a wide range, from 5.82 to 7636 ppm at Talatui, from 67.82 to 9105 ppm in Teremkyn pyrite, and from 0.61 to 10,360 ppm in pyrite from Darasun (Table 2). Although the geometric means of As content in pyrites from Teremkyn and Darasun do not show a strong correlation with temperature, as is the case with Co, we believe this is due to a smaller set of data on the Teremkyn pyrite.

Table 2. Compilation of LA-ICP-MS analyses (ppm) for trace element of pyrite from Talatui, Teremkyn, and Darasun deposits.

Deposit	n	Parameter	Co	Ni	Cu	Zn	As	Se	Ag	In	Sb	Te	W	Au	Pb	Bi
Talatui	152	Median	541.5	40.05	18.1	13.51	204	51.8	3.76	1.56	0.95	8.86	1.55	0.87	1.79	1.85
		GM	309.5	39.72	20.43	15.24	185.3	52.64	3.08	0.78	1.59	8.69	1.2	0.82	2.23	1.62
		Min	0.6	2.67	1.59	5.13	5.82	17.3	0.24	0.21	0.41	2.08	0.05	0.13	0.21	0.06
		Max	20559	3647	3257	176.2	7636	134.6	46.46	2.92	36.85	44.38	89.18	6.78	347.1	79.03
		n*	149	139	87	31	151	60	68	2	24	18	15	19	115	104
		GSD	29.67	4.58	3.36	3.47	16.51	7.91	0.45	0.16	0.35	2.05	0.57	0.19	0.4	0.31
Teremkyn	29	Median	70.25	299.6	4.68	13.24	1132	-	4.22	-	0.81	8.68	-	0.3	12.12	12.28
		GM	74.83	148.4	10.65	13.24	643.2	-	3.69	-	1.45	7.72	-	0.74	11.71	7.29
		Min	3.95	2.05	1.87	13.24	67.82	-	0.11	-	0.52	2.08	-	0.15	0.72	0.06
		Max	5607	913.1	165.5	13.24	9105	-	45.39	-	15.91	24.35	-	6.94	662.2	496.6
		n*	28	26	20	1	29	-	11	-	8	18	-	10	25	21
		GSD	6.57	13.43	1.99	3.63	42.98	-	0.77	-	0.29	1.87	-	0.16	2.2	1.48
Darasun	112	Median	24.56	16.5	45.39	395.2	735.6	26.01	3.14	6.49	2.02	7.48	0.93	0.87	12.31	6.73
		GM	24.03	26.9	49.2	314	423.8	28.15	3.71	5.86	2.31	8.49	0.64	0.85	18.04	8.91
		Min	0.49	2.11	4.01	5.34	0.61	15.01	0.12	0.23	0.46	2.03	0.23	0.1	0.39	0.08
		Max	3231	1232	19491	10466	10360	89.71	304.4	44.64	26.17	50.2	1.22	21.95	21734	2350
		n*	58	57	99	45	104	29	78	32	62	31	3	29	72	73
		GSD	3.67	3.83	6.51	53.54	42.72	3.86	0.63	0.98	0.41	1.82	0.11	0.13	2.53	1.51
		Median detection limits	0.3	2	1.5	5	3	15	0.1	0.04	0.4	2	0.03	0.1	0.2	0.03

Note: GM—geometric mean, GSD—geometric standard deviation, n—number of analyses, n*—number of analyses above the detection limit, n.a.—not analyzed as major component, "-"—below detection limit.

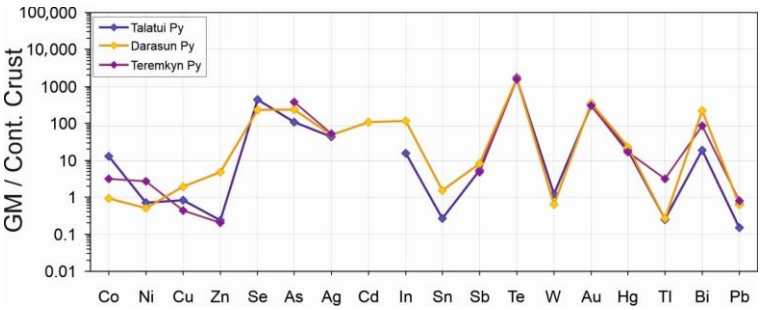

Figure 6. Multi-element diagram for pyrite (Py) from the Talatui, Teremkyn, and Darasun ores, normalized to the bulk continental crust [34]. GM—geometric means (Table 2) calculated from data presented in Table S2.

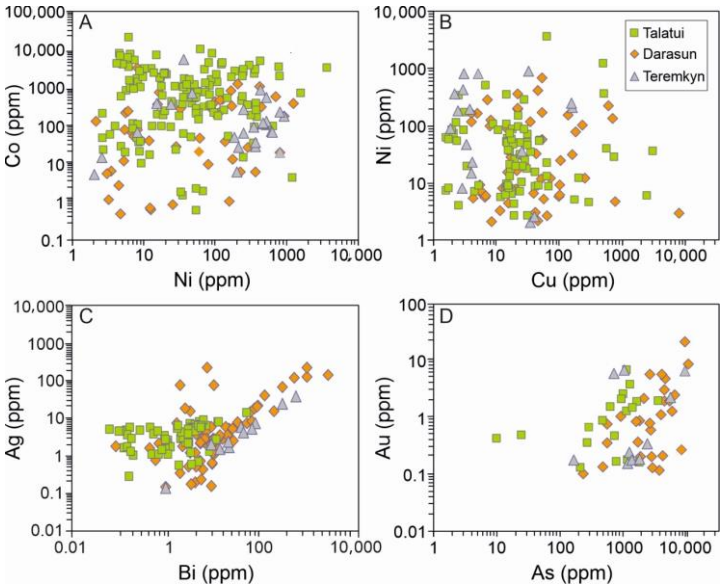

Figure 7. Trace element variation diagrams of pyrite from Talatui, Teremkyn, and Darasun ores for (**A**)—Co vs. Ni, (**B**)—Ni vs. Cu, (**C**)—Ag vs. Bi, and (**D**)—Au vs. As.

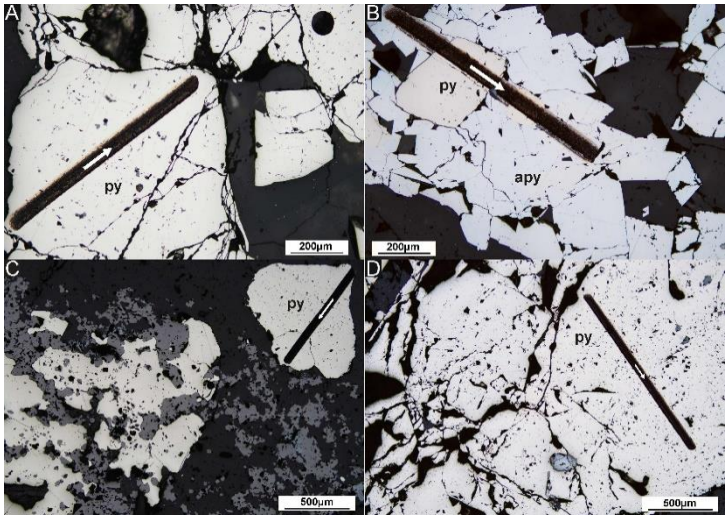

Figure 8. Photomicrographs of the LA-ICP-MS profiles in pyrite from Darasun (**A**,**B**), Talatui (**C**), and Teremkyn (**D**) ores in reflected light. A—LA-ICP-MS profile through an euhedral pyrite grain from sample 6Vd89. B—profile through pyrite grains in arsenopyrite from sample 6Vd89. C—profile in a distinct anhedral pyrite grain from sample 50-01. D—profile in pyrite aggregate from sample 2415Sht.

Pyrite from the Teremkyn deposit accommodates Ni in a mean concentration of 299.6 ppm, while the Darasun and Talatuy pyrites are relatively depleted in Ni (Figure 6; Table 2). Copper and zinc as well as arsenic are concentrated mostly in the middle-temperature pyrite from the Darasun deposit than in the high-temperature Talatui pyrite. The lowest median concentrations of Cu were detected in the Teremkyn pyrite (Figure 7B; Table 2). Zinc also shows a strong correlation with Ag, Bi, and Sb in LA-ICP-MS profiles of the Darasun pyrite. Except for a few analyses (Figure 7C), pyrites from all deposits have similar concentrations of Ag; however, Ag concentrations are different in other minerals. Furthermore, the Darasun pyrite contains much higher concentrations of In, Sn, Au, Pb, and Bi and lower contents of W than the Talatui pyrite (Figure 6; Table 2). The maximum content of Sn (22 ppm) was detected in the Darasun pyrite, which is also enriched in Sn and

In, and these elements demonstrate a positive correlation with one another in all analyses of the Darasun pyrite (Table S2).

Pyrite from the Darasun deposit is characterized by the highest gold concentrations compared to pyrite at the others deposits (Table 2). To avoid a possible influence of gold micro-inclusions on the bulk composition, we carefully identified each time-resolved spectrum and recognized several distributional patterns in gold accommodation. Microphotographs of the LA-ICP-MS profiles in the ores are presented in Figure 9, and the spectra for these profiles are shown in Figure 8. In the high-temperature pyrite from the Talatui deposit, Au, Bi, and Te form distinct peaks regardless of the As concentration (Figure 9C). However, arsenic contents in the middle-temperature Darasun and Teremkyn pyrite correlate with Au (Figure 9A,B). Gold in the Teremkyn pyrite shows a strong correlation with As, Ag, Sb, and Bi (Figure 9B).

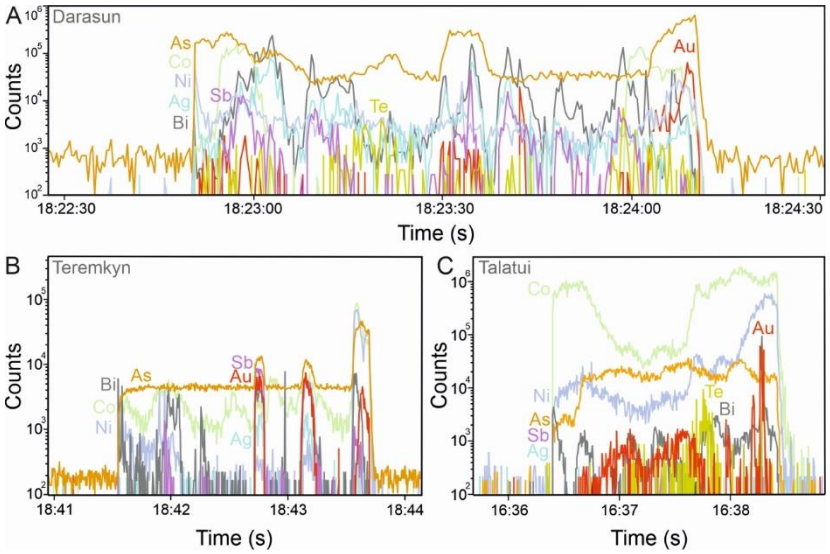

Figure 9. Time-resolved signal counts for trace elements for LA-ICP-MS profiles in pyrite from the Darasun (**A**, Figure 8A), Teremkyn (**B**, Figure 8D) and Talatui (**C**, Figure 8C) deposits.

The Darasun pyrite does not show any clear correlations between Au, Ag, Sb, and Bi distributions (Figure 9A). Gold is distributed heterogeneously and sometimes forms peaks and zones of enrichment together with these elements but mostly seems to be independent. Silver and Bi correlate with each other and, to a lesser extent, with Sb and Au. A direct correlation between Ag and Bi and between Au and As in the middle-temperature pyrites is also clearly seen on Figure 7C,D.

5. Discussion

In interpreting our data, we proceeded from the hypothesis that the Darasun goldfield was formed by a single (united) fluid–magmatic system. It has been demonstrated above that the age of the intrusive granitoid massif coincides with the age of wall-rock metasomatites at the Darasun deposit [21]. Detailed published isotope data prove the magmatic nature of the source of mineralizing fluid at the Darasun deposit [32]. The three deposits occur at different distances from the granitoid massif, and their spatial distribution should have controlled differences between the temperatures at which their gold mineralization was formed. Indeed, data on mineral-hosted fluid inclusions indicate that despite the general similarities between the physicochemical parameters and compositions of the mineralizing fluids, they show some differences: the maximum and mean temperatures of the mineral-forming processes systematically decrease from the Talatui deposit to the Darasun one [18,20,26,27,29]. These variations are associated with those in compositional features of some minerals at the same deposits [18,28] at the generally similar mineralogy of ores at these deposits. This stimulated us to search for differences in the accumulation of

trace elements in pyrite from the gold ores of the deposits. We believe these differences should have been controlled first by the crystallization temperature.

According to the principal goal of this study, we found concentrations of some trace elements in pyrite deposited in various parts of the fluid–magmatic system show correlations with the variations in the pyrite crystallization temperature. The concentrations of some trace elements (Cu, Zn, Ag, Te, and As,) in the pyrite monotonously increase with the transition from the mineral of the Talatui deposit to that of the Teremkyn and then Darasun deposits, i.e., with a temperature decrease. Another element that belongs to this group is In, whose concentrations have not been analyzed in the ores of the Teremkyn deposits. It is pertinent to mention the publication [35] in which the example of a modern geothermal system is employed to show that higher concentrations of Co and Ni and relatively low concentrations of As, Cu, Pb, Ag, and Au in pyrite may be indicators of boiling. In our situation, we cannot estimate how boiling affected the concentrations of these elements in the pyrite because the evidence for boiling has been found at all three deposits.

Some other elements show another temperature dependence of their concentrations: concentrations of these elements in pyrite decrease from the Talatui deposit to the Teremkyn and then to Darasun ones. These elements are Co, Se, and W, although data on concentrations of Se and W in the pyrite from Teremkyn are absent. They are regarded to be below the detection limit. The concentrations of the other five elements (Ni, Au, Bi, Sb, and Pb) do not linearly correlate with the pyrite crystallization temperature.

To test the aforementioned trends in concentrations of trace elements in the pyrite, we constructed boxplot diagrams, which are used to compare sets of significantly different data and enable one to clearly illustrate trends and relations identified by means of statistical analysis (Figures 10–12). This allowed us to confidently conclude the principal factor controlling concentrations of many trace elements (Cu, Zn, Ag, Sb, Pb, In, Co, Te, Se, and W) in pyrite in fluid–magmatic systems is temperature. This property of the elements can be used in studying the Au-Bi mineralization of the intrusion-related type. However, at this stage, it is too early to judge whether the found dependences are direct or mediated. The mechanism of the effect of temperature on the concentration of these trace elements in such multifactorial systems [36] requires special experimental studies, which may be stimulated by the publication of our results.

The behaviors of elements whose concentrations are not controlled by temperature may be explained by various processes and phenomena, for example, some local fluctuations in the composition of the fluid or host rocks. For instance, the high Ni concentrations in pyrite from the Teremkyn deposit may be explained by the gold mineralization of this deposit is hosted in gabbroic rocks, which were enriched in Ni during the magmatic stage. Gold concentration in pyrite at the Darasun ore field has been experimentally demonstrated [37] to be much lower than when pyrite crystallized from Au-saturated hydrothermal fluid. The pyrite may have later recrystallized under the effect of an Au-poor solution.

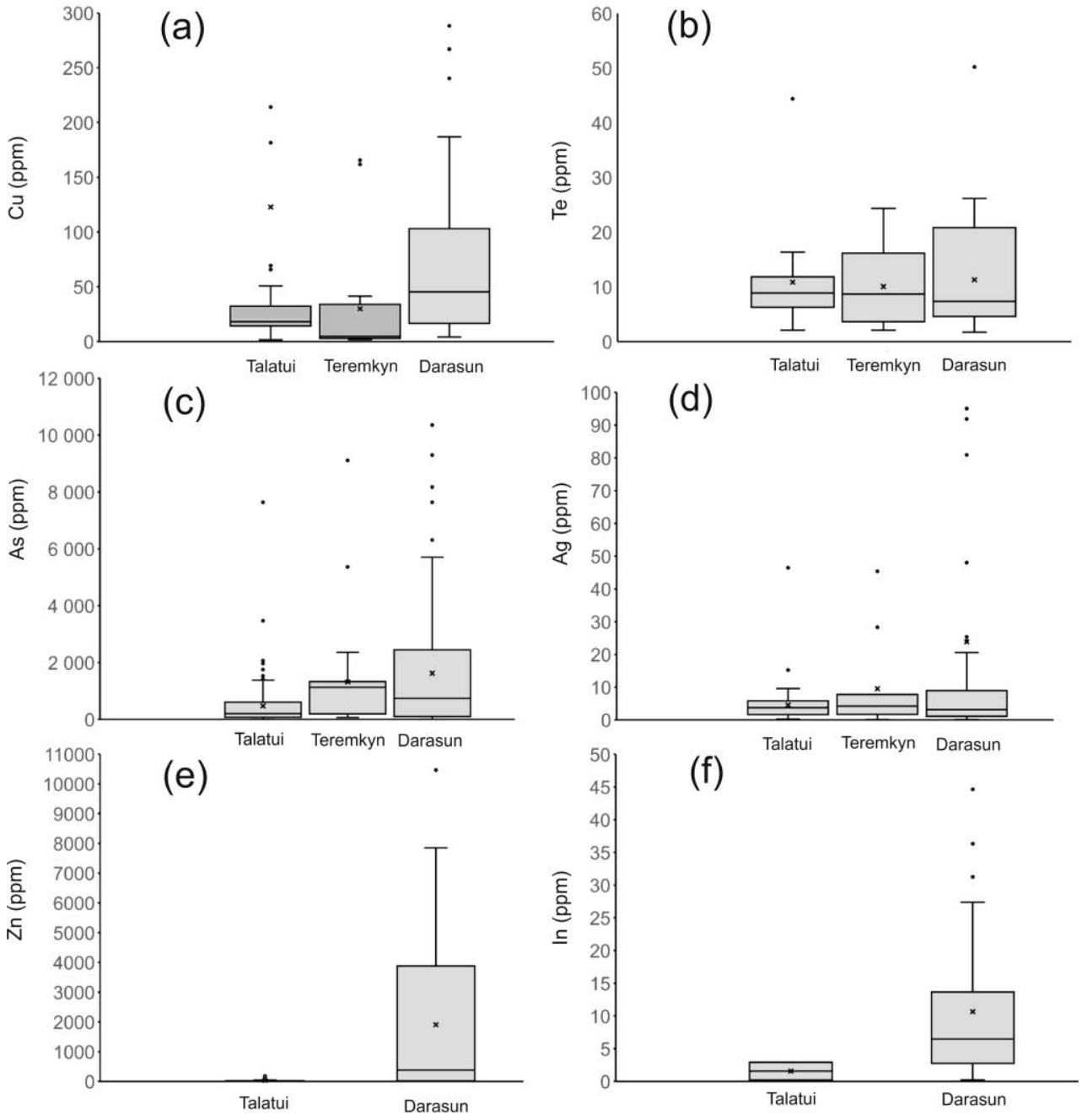

Figure 10. Boxplot diagrams of elements whose concentrations increase with a temperature decrease: (**a**)—Cu, (**b**)—Te, (**c**)—As, (**d**)—Ag, (**e**)—Zn, (**f**)—In.

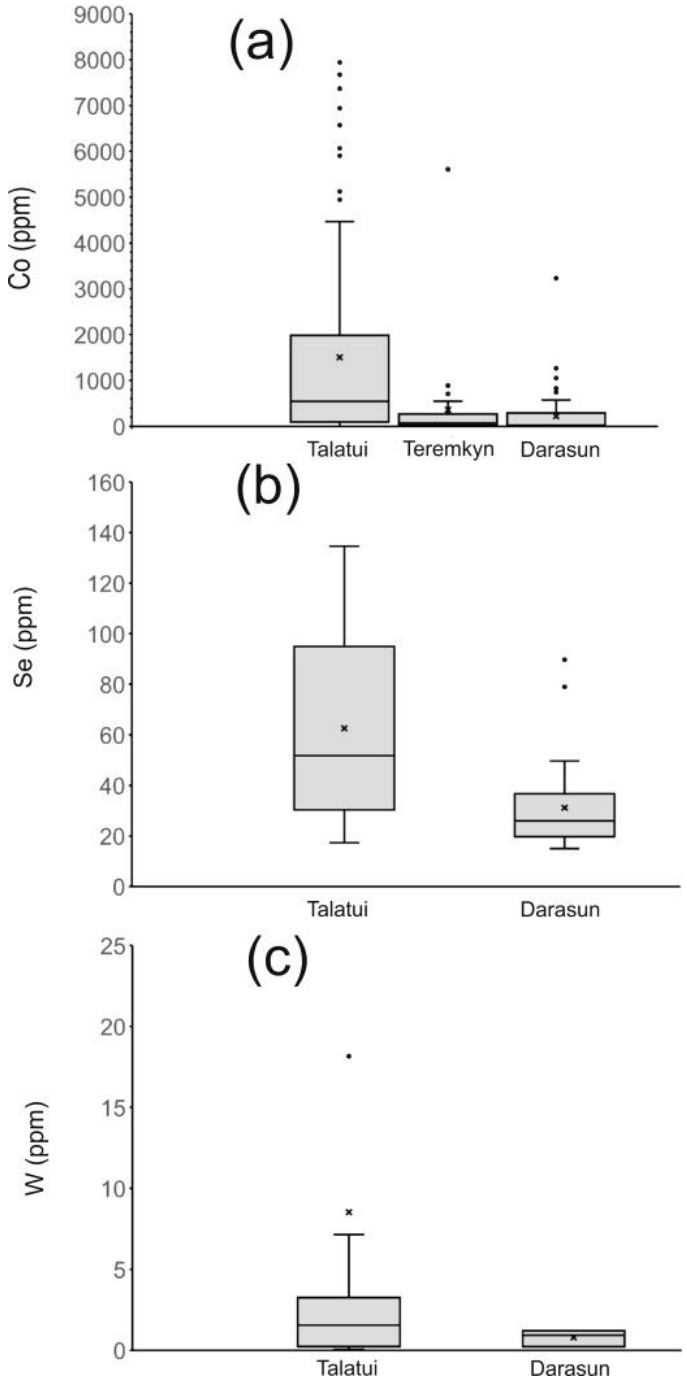

Figure 11. Boxplot diagrams of elements whose concentrations decrease with a temperature decrease: (**a**)—Co, (**b**)—Se, (**c**)—W.

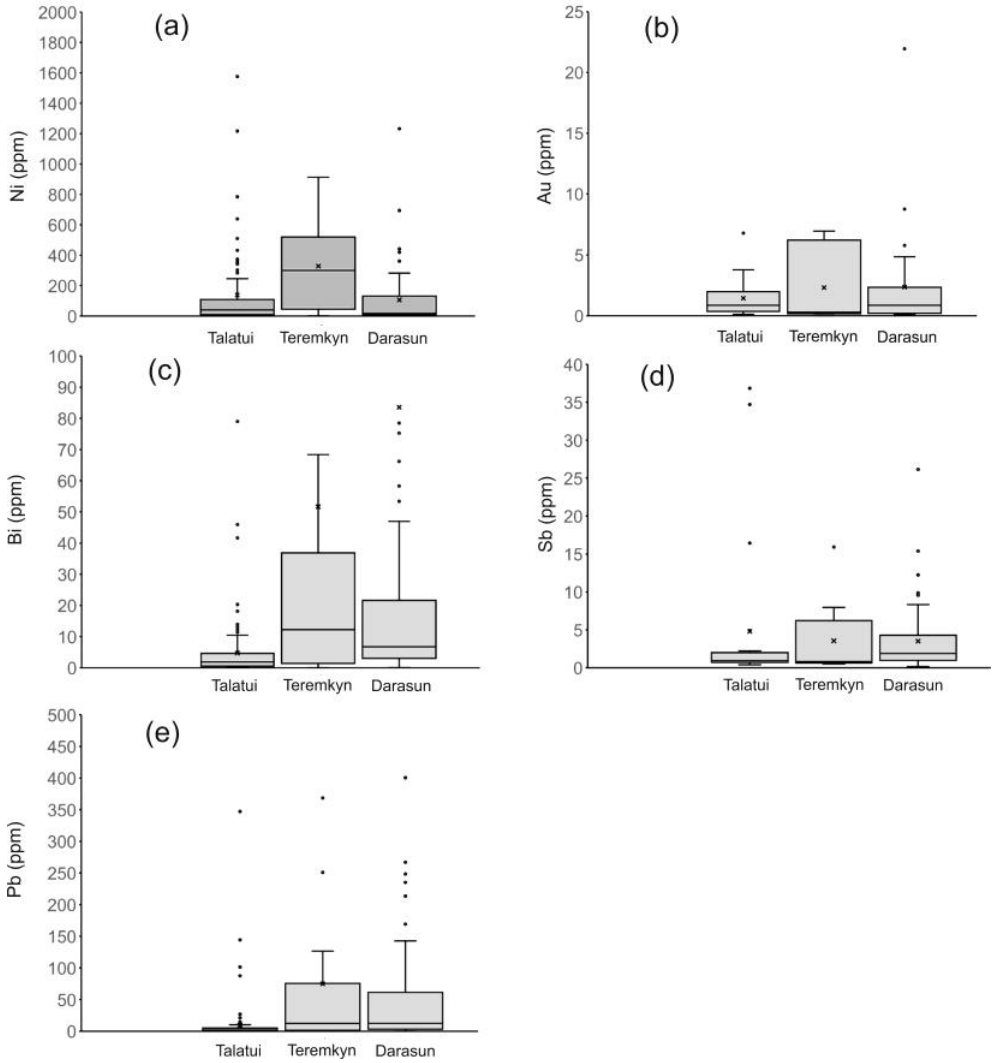

Figure 12. Boxplot diagrams of elements whose concentrations show no relation to the temperature changes: (**a**)—Ni, (**b**)—Au, (**c**)—Bi, (**d**)—Sb, (**e**)—Pb.

6. Conclusions

Concentrations of trace elements have been analyzed in pyrite from gold ores from the Darasun goldfield. These ores were formed by the single fluid–magmatic system at different temperatures. We determined Co, Se, and W were enriched in the high-temperature pyrite, whereas Cu, Zn, Ag, Te, As, and In were accumulated in the medium-temperature pyrite. The behavior of some elements (Ni, Au, Bi, Sb, and Pb) did not show any temperature dependence and hence, was likely controlled by some other factors. The relations and trends identified in the behavior of the elements can be used when the Au-Bi mineralization of the intrusion-related type is studied.

Supplementary Materials: The following supporting information can be downloaded at: https://www.mdpi.com/article/10.3390/min13020288/s1, Table S1: Concentrations of trace elements (ppm) in sulfides from Darasun, Talatuy, and Teremki by LA-ICP-M; Table S2: The results of the RSM measurements for estimation of accuracy and precision of the LA-ICP-MS analysis.

Author Contributions: Conceptualization, V.P. and N.B.; methodology, V.P.; software, V.A.; validation, V.P., V.B. and V.A.; formal analysis, V.P.; investigation, V.P.; resources, V.P., L.Z. and A.K.; data curation, V.P.; writing—original draft preparation, V.P. and V.B.; writing—review and editing, V.P.; visualization, V.P.; supervision, V.P.; project administration, N.B.; funding acquisition, V.P. All authors have read and agreed to the published version of the manuscript.

Funding: This research was supported by the Ministry of Education and Science of the Russian Federation, project no. 075-15-2020-802.

Data Availability Statement: Not applicable.

Acknowledgments: LA ICP MS analyses were made at the IGEM-Analitka Research Center.

Conflicts of Interest: The authors declare no conflict of interest.

References

1. Cook, N.J.; Ciobanu, C.L.; Mao, J. Textural control on gold distribution in as-free pyrite from the Dongping, Huangtuliang and Hougou gold deposits, north China craton (Hebei province, China). *Chem. Geol.* **2009**, *264*, 101–121. [CrossRef]
2. Koglin, N.; Frimmel, H.E.; Minter, W.L.; Brätz, H. Trace-element characteristics of different pyrite types in Mesoarchaean to Palaeoproterozoic placer deposits. *Miner. Deposita* **2010**, *45*, 259–280. [CrossRef]
3. Reich, M.; Deditius, A.; Chryssoulis, S.; Li, J.-W.; Ma, C.-Q.; Parada, M.A.; Barra, F.; Mittermayr, F. Pyrite as a record of hydrothermal fluid evolution in a porphyry copper system: A SIMS/EMPA trace element study. *Geochem. Cosmochim. Acta* **2013**, *104*, 42–62. [CrossRef]
4. Deditius, A.P.; Reich, M.; Kesler, S.E.; Utsunomiya, S.; Chryssoulis, S.L.; Walshe, J.; Ewing, R.C. The coupled geochemistry of Au and as in pyrite from hydrothermal ore deposits. *Geochim. Cosmochim. Acta* **2014**, *140*, 644–670. [CrossRef]
5. Gregory, D.D.; Large, R.R.; Bath, A.B.; Steadman, J.A.; Wu, S.; Danyushevsky, L.; Bull, S.W.; Holden, P.; Ireland, T.R. Trace element content of pyrite from the kapai slate, St. Ives Gold District, Western Australia. *Econ. Geol.* **2016**, *111*, 1297–1320. [CrossRef]
6. Tardani, D.; Reich, M.; Deditius, A.P.; Chryssoulis, S.; Sánchez- Alfaro, P.; Wrage, J.; Roberts, M.P. Copper-arsenic decoupling in an active geothermal system: A link between pyrite and fluid composition. *Geochem. Cosmochim. Acta* **2017**, *204*, 179–204. [CrossRef]
7. Xie, J.; Ge, L.; Qian, L.; Li, Q.; Sun, W. Trace element characteristics of pyrite in Dongguashan Cu (Au) deposit, Tongling region, China. *Solid Earth Sci.* **2020**, *5*, 233–246. [CrossRef]
8. Large, R.R.; Danyushevsky, L.V.; Hollit, C.; Maslennikov, V.; Meffre, S.; Gilbert, S.E.; Bull, S.; Scott, R.J.; Emsbo, P.; Thomas, H.; et al. Gold and trace element zonation in pyrite using a laser imaging technique: Implications of the timing of gold in orogenic and Carlin-style sediment-hosted deposits. *Econ. Geol.* **2009**, *104*, 635–668. [CrossRef]
9. Deol, S.; Deb, M.; Large, R.R.; Gilbert, S. LA-ICPMS and EPMA studies of pyrite, arsenopyrite and loellingite from the Bhukia-Jagpura gold prospect, southern Rajasthan, India: Implications for ore genesis and gold remobilization. *Chem. Geol.* **2012**, *326–327*, 72–87. [CrossRef]
10. King, J.; Williams-Jones, A.E.; Hinsberg, V.V.; Willians-Jones, G. High-sulfidation epithermal pyrite-hosted Au (Ag-Cu) ore formation by condensed magmatic vapors on sangihe island, Indonesia. *Econ. Geol.* **2014**, *109*, 1705–1733. [CrossRef]
11. Keith, M.; Häckel, F.; Haase, K.M.; Schwarz-Schampera, U.; Klemd, R. Trace element systematics of pyrite from submarine hydrothermal vents. *Ore Geol. Rev.* **2016**, *72*, 728–745. [CrossRef]
12. Keith, M.; Haase, K.M.; Klemd, R.; Krumm, S.; Strauss, H. Systematic variations of trace element and sulfur isotope compositions in pyrite with stratigraphic depth in the Skouriotissa volcanic-hosted massive sulfide deposit, Troodos ophiolite, Cyprus. *Chem. Geol.* **2016**, *423*, 7–18. [CrossRef]
13. Mukherjee, I.; Large, R. Application of pyrite trace element chemistry to exploration for SEDEX style Zn-Pb deposits: McArthur Basin, Northern Territory, Australia. *Ore Geol. Rev.* **2017**, *81*, 1249–1270. [CrossRef]
14. Keith, M.; Smith, D.J.; Jenkin, G.R.T.; Holwell, D.A.; Dye, M.D. A review of Te and Se systematics in hydrothermal pyrite from precious metal deposits: Insights into ore-forming processes. *Ore Geol. Rev.* **2018**, *96*, 269–282. [CrossRef]
15. Gregory, D.D.; Cracknell, M.J.; Large, R.R.; McGoldrick, P.; Kuhn, S.; Maslennikov, V.V.; Baker, M.J.; Fox, N.; Belousov, I.; Figueroa, M.C.; et al. Distinguishing ore deposit type and barren sedimentary pyrite using laser ablation-inductively coupled plasma-mass spectrometry trace element data and statistical analysis of large data sets. *Econ. Geol.* **2019**, *114*, 771–786. [CrossRef]
16. Xie, J.C.; Ge, L.K.; Fang, D.; Li, Q.Z.; Qian, L.; Li, Z.S.; Yan, J.; Sun, W.D. Geochemistry of pyrite from stratabound massive sulfide deposits, Tongling region, China: Implication for their genesis. *Ore Geol. Rev.* **2020**, *120*, 103430. [CrossRef]
17. Xie, J.C.; Tang, D.W.; Qian, L.; Wang, Y.; Sun, W.D. Geochemistry of sulfide minerals from skarn Cu (Au) deposits in the Fenghuangshan ore field, Tongling, eastern China: Insights into ore-forming process. *Ore Geol. Rev.* **2020**, *122*, 103537. [CrossRef]
18. Prokofiev VYu Garofalo, P.S.; Bortnikov, N.S.; Kovalenker, V.A.; Zorina, L.D.; Grichuk, D.V.; Selektor, S.L. Fluid Inclusion Constraints on the Genesis of Gold in the Darasun District (Eastern Transbaikalia), Russia. *Econ. Geol.* **2010**, *105*, 395–416. [CrossRef]
19. Timofeyevsky, D.A. *Geology and Mineralogy of the Darasun Gold Area*; Nedra Publisher: Moscow, Russia, 1972; p. 260. (In Russian)
20. Prokofiev, V.Y.; Bortnikov, N.S.; Zorina, L.D. Genetic features of the Darasun gold-sulphide deposit (eastern Transbaikal region, Russia). *Geol. Ore Depos.* **2000**, *42*, 526–548.
21. Chernyshev, I.V.; Prokofiev, V.Y.; Bortnikov, N.S.; Chugaev, A.V.; Goltsman, Y.V.; Lebedev, V.A.; Larionova, Y.O.; Zorina, L.D. Age of Granodiorite Porphyry and Beresite from the Darasun Gold Field, Eastern Transbaikal Region, Russia. *Geol. Ore Depos.* **2014**, *56*, 1–14. [CrossRef]

22. Rutshtein, I.G.; Chaban, N.N. Geological Structure of the Chita District. In *Explanatory Note to the Geological Map on a Scale 1:500,000*; Komitet po geologii i ispol'zovaniyu nedr Chit. Obl. Publisher: Chita, Russia, 1997; p. 239. (In Russian)
23. Sakharova, M.S. The gold mineralogy of the Darasun deposit (eastern Transbaikal region). *Izv. Akad. Nauk. USSR Geol. Ser.* **1968**, *11*, 51–68. (In Russian)
24. Lyakhov, Y.V. Temperature Zoning of the Darasun Deposit. *Geol. Rudn. Mestorozhd.* **1975**, *75*, 28–36.
25. Prokofiev, V.Y.; Zorina, L.D.; Kovalenker, V.A.; Akinfiev, N.N.; Baksheev, I.A.; Krasnov, A.N.; Yurgenson, G.A.; Trubkin, N.V. Composition, formation conditions, and genesis of the Talatui gold deposit, the eastern Transbaikal region, Russia. *Geol. Ore Depos.* **2007**, *49*, 31–68. [CrossRef]
26. Prokofiev, V.Y.; Zorina, L.D.; Baksheev, I.A.; Plotinskaya, O.Y.; Kudryavtseva, O.E.; Ishkov, Y.M. Minerals and formation conditions of ores of the Teremkin gold deposit (eastern Transbaikal region, Russia). *Geol. Ore Depos.* **2004**, *46*, 332–352.
27. Prokofiev, V.Y.; Bortnikov, N.S.; Kovalenker, V.A.; Vinokurov, S.F.; Zorina, L.D.; Chernova, A.D.; Kryazhev, S.G.; Krasnov, A.N.; Gorbacheva, S.A. The Darasun Gold Deposit, Eastern Transbaikal Region: Chemical Composition, REE Patterns, and Stable Carbon and Oxygen Isotopes of Carbonates from Ore Vein. *Geol. Ore Depos.* **2010**, *52*, 81–113. [CrossRef]
28. Prokofiev, V.Y.; Bortnikov, N.S.; Kovalenker, V.A.; Zorina, L.D.; Baksheev, I.A.; Grichuk, D.V.; Krasnov, A.N.; Selector, S.L. Vertical mineralogical-geochemical zoning of Mesozoic Transbaikalia fluid-magmatic gold systems. In *Large igneos Provinces of Asia, Mantle Plumes and Metallogeny, Proceedings of the International Symposium, Novosibirsk, Russia, 6–9 August 2009*; Nauka: Novosibirsk, Russia, 2009; pp. 251–254.
29. Prokofiev, V.Y.; Selector, S.L. Fluid inclusion evidence for barbotage and its role in gold deposition at the Darasun goldfield (eastern Transbaykalia, Russia). *Cent. Eur. J. Geosci.* **2014**, *6*, 131–138. [CrossRef]
30. Savard, D.; Bouchard-Boivin, B.; Barnes, S.-J.; Garbe-Schönberg, D. UQAC-FeS: A new series of base metal sulfide quality control reference material for LA-ICP-MS analysis. In Proceedings of the 10th International Conference on the Analysis of Geological and Environmental Materials, Sydney, Australia, 8–13 July 2018.
31. Garbe-Schönberg, D.; Müller, S. Nano-particulate pressed powder tablets for LA-ICP-MS. *J. Anal. At. Spectrom.* **2014**, *29*, 990–1000. [CrossRef]
32. Paton, C.; Hellstrom, J.; Paul, B.; Woodhead, J.; Hergt, J. Iolite: Freeware for the visualisation and processing of mass spectrometric data. *J. Anal. At. Spectrom.* **2011**, *26*, 2508–2518. [CrossRef]
33. Abraitis, P.K.; Pattrick, R.A.D.; Vaughan, D.J. Variations in the compositional, textural and electrical properties of natural pyrite: A review. *Int. J. Miner. Process.* **2004**, *74*, 41–59. [CrossRef]
34. Wedepohl, K.H. The Composition of the Continental Crust. *Geochim. Et Cosmochim. Acta* **1995**, *59*, 1217–1232. [CrossRef]
35. Nelson, R.; Reich, M.; Leisen, M.; Morata, D.; Barra, F.; Deditius, A.P. Geochemical and micro-textural fingerprints of boiling in pyrite. *Geochim. Et Cosmochim. Acta* **2019**, *246*, 60–85. [CrossRef]
36. Smagunov, N.; Tauson, V.; Lipko, S.; Babkin, D.; Pastushkova, T.; Belozerova, O.; Bryansky, N. Partitioning and Surficial Segregation of Trace Elements in Iron Oxides in Hydrothermal Fluid Systems. *Minerals* **2021**, *11*, 57. [CrossRef]
37. Prokofiev, V.Y.; Tagirov, B.R.; Brovchenko, V.D.; Reukov, V.L.; Filimonovaa, O.N.; Zorina, L.D.; Abramova, V.D.; Kovalchuk, E.V.; Mezhueva, A.A.; Nikolaeva, I.Y.; et al. Gold in Natural and Synthetic Pyrite: A Case of the Darasun Gold District, Eastern Transbaikal Region, Russia. *Geol. Ore Depos.* **2022**, *64*, 329–349. [CrossRef]